This is an open access article published under an ACS AuthorChoice License, which permits copying and redistribution of the article or any adaptations for non-commercial purposes.

ACS OMEGA

http://pubs.acs.org/journal/acsodf

Article

Fabrication of Nanofibrous/Xerogel Layer-by-Layer Biocomposite Scaffolds for Skin Tissue Regeneration: In Vitro Study

Fatma Elshishiny and Wael Mamdouh*

Cite This: *ACS Omega* 2020, 5, 2133−2147

Read Online

ACCESS | Metrics & More | Article Recommendations

ABSTRACT: Skin burn wounds are a crucial issue that could reduce life quality. Although numerous effective skin products have invaded the biomedical market, most of them still demonstrate some limitations regarding their porosity, swelling and degradation behaviors, antibacterial properties, and cytotoxicity. Thus, the aim of this study is to fabricate novel trilayered asymmetric porous scaffolds that can mimic the natural skin layers. In particular, the fabricated scaffold constitutes an upper electrospun chitosan−poly(vinyl alcohol) layer and a lower xerogel layer, which is made of effective skin extracellular matrix components. Both layers are fixed together using fibrin glue as a middle layer. The results of this study revealed promising scaffold swelling capability suitable for absorbing wound exudates, followed by a constant degradable weight over time, which is appropriate for a burn wound environment. Scanning electron microscopy images revealed an average pore diameter in the range of 138.39−170.18 nm for the cross-linked electrospun mats and an average pore size of 2.29−30.62 μm for the fabricated xerogel layers. This further provided an optimum environment for fibroblast migration and proliferation. The electrospun nanofibrous layer was examined for its antibacterial properties and showed expressive complete bacterial inhibition against Gram-positive (*Staphylococcus aureus*) and Gram-negative (*Escherichia coli*) bacterial strains (log reduction = 3 and 2.70, respectively). Next, mouse embryonic fibroblast cytotoxicity and migration rate were investigated against the developed asymmetrical composite to assess its biocompatibility. Tissue culture experiments demonstrated significant cell proliferation and migration in the presence of the constructed scaffold ($P < 0.0001$). A complete wound closure was observed in vitro in the presence of the three scaffold asymmetrical layers against the mouse embryonic fibroblast. The results of this study proved superior biological characteristics of the innovative asymmetrical composite that could further replace the burned or damaged skin layers with promising potential for clinical applications.

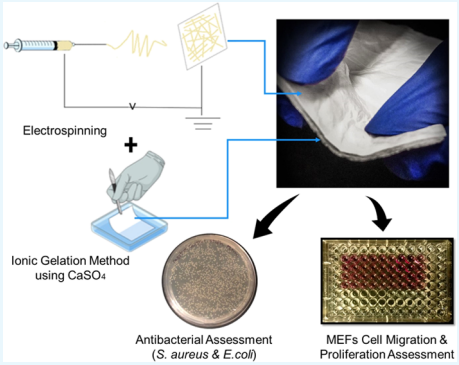

1. INTRODUCTION

Skin plays a substantial role in the protection process against the surrounding external environment. Loss of healthy skin integrity leads to a lack of the physiological homeostasis of the whole body. In the past decade, burn wounds were increased dramatically, with about 180 000 global deaths annually. The majority of these burn cases took place in low- and middle-income countries, according to the World Health Organization.[1] Moreover, the Center for Disease Control in the USA determined the annual statistics in the USA to about 1.1 million people who experienced burn injuries and demanded intensive medical care. Roughly, 50 000 of these patients required hospitalization and 20 000 underwent major burns with around 25% loss of their skin body surface. Unfortunately, this in most cases could lead to disability-adjusted life years and cause of death. Almost 4500 patients with severe burns are most likely to die and 10 000 could die because of burn-related infections. These data are alarming for the distressing consequences of burn injury burden to patients and the responsible authorities worldwide.[2]

Chronic burn wounds, especially the third-degree burns, have more harmful consequences on affected patients than other wound types. This difference is mainly related to their specific related three distinctive zones, which are known as Jackson's burn wound zones.[3] The first zone is the coagulation zone, which experiences the maximum point of tissue damage with permanent loss of its tissue due to the coagulation of the constitutive proteins. After that, it is followed by the zone of stasis, which is encircling the coagulation zone and acts as a salvageable.[3,4] Thus, effective management of burns is important here to help increasing tissue perfusion and hinder any possibility of irreversible tissue loss. The third outward zone is the zone of hyperemia, in which the tissue perfusion is high and tissue repair is constantly taking place in the absence of unfavorable factors like sepsis or hypoperfusion. These

Received: September 2, 2019
Accepted: January 20, 2020
Published: January 31, 2020

© 2020 American Chemical Society

https://dx.doi.org/10.1021/acsomega.9b02832
ACS Omega 2020, 5, 2133−2147

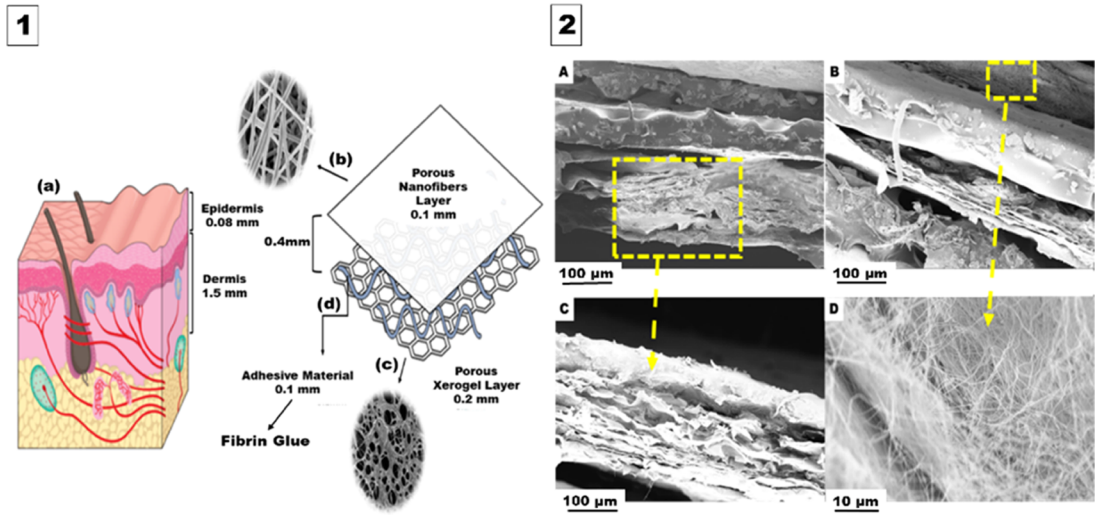

Figure 1. Engineered design of the trilayered asymmetric porous biocomposite scaffold. (1) Hypothesized design. (2) Cross section of the fabricated asymmetrical scaffold. (1A) Normal human skin layers. (1B) Upper layer consists of a porous nanofibrous sheet with an average thickness of 0.1 mm. (1C) Lower layer constitutes a xerogel mat with an average thickness of 0.2 mm. (1D) Middle fibrin glue layer (0.1 mm). (2A) and (2B) Cross sections of the complete scaffold layers at two different regions from the tested sample under the scanning electron microscopy (SEM). (2C) Individual cross section of the produced lower xerogel layer. (2D) Upper surface of the nanofiber (NF) layer.

zones are three dimensional, and the most critical one is the zone of stasis, as inappropriate resuscitation would increase the severity of the burn wound.[3] The perfect scaffold should connect the living tissues that lay on the burn wound edges and act as a bridge for epithelial migration. Besides that, it should protect against bacterial pathogens and absorb wound exudates. Meanwhile, it must be biodegradable, biocompatible, and comprise an optimum microspore structure.[5]

From old days, applications of saline-soaked gauzes and split-thickness or full-thickness skin grafts have been the golden standard techniques according to the underlying burn wound condition. The primary aim of burnt area treatment is to avoid infection and provide a rapid healing process in as shorter time as possible. However, those conventional methods may display unpleasant outcomes that can result in late wound closure and high bacterial invasion.[6−8] Several artificial skin products have invaded the market, either by combining with the standard grafting procedure or being embedded with cultured cells to enhance the treatment of chronic burn wounds. Nevertheless, such complex biological skin equivalents result in improved burn wound healing; however, they demonstrate a wide range of drawbacks in terms of cytotoxicity, invasion of pathogens, and their high cost of production.[9,10]

Biopolymers are being used in diverse biomedical applications, as they provide a favorable and natural environment for cell proliferation and migration. Moreover, it is critical to utilize biodegradable and biocompatible components when it comes to the fabrication of artificial skin substitutes alongside seeding of the main skin cell types (e.g., fibroblasts and keratinocytes), which can result in rapid skin regeneration in case of burn wounds. Numerous experiments have been conducted on the potential biomaterial-based scaffolds in skin tissue engineering.[11] One contemporary study has fabricated a porous collagen scaffold using different variants of lyophilized type I collagen solution; meanwhile, different ratios of a collagen−agarose mixture solution have been used to fabricate the other three comparable scaffolds.

The morphological characterization showed a microporous structure with a porosity of 99.15% for the collagen scaffold and more than 98% in all other tested variants. The scaffolds showed considerable biocompatibility and biodegradability when tested on fibroblast cell lines with excellent cell morphology and viability with enhanced structural properties upon the addition of agarose. The previous examples could explain the potential of collagen-based scaffolds in the engineering of various organs including the skin.[12]

In this study, polysaccharides [chitosan (Cs) and alginate] and proteins [collagen, gelatin, elastin (El.), and fibrinogen] were used due to their high cytocompatibility and biodegradability, nontoxicity, and antioxidant, antimicrobial, and antifungal properties.[12−17] These biopolymers involve proteins such as collagen type I, which demonstrates around 80−85% of the skin extracellular matrix (ECM) and provides favorable cell interactive properties. Elastin represents around 1−2% of the total dermal proteins and exhibits a vital role in providing unique physiological elasticity for several connective tissues including skin, lungs, and blood vessels.[18] Fibrin glue, which plays a definitive role in the blood coagulation cascade, besides its golden ability to act as a hemostatic barrier, serves as a scaffold for cell migration and has been used as a tissue adhesive for a variety of human surgical procedures.[19−21] Gelatin illustrates significant properties that are close to those of collagen type I since it contains the typical amino acids present in collagen, besides its ability to form a gel at decreased temperatures in the range of 20−30 °C.[13,22−24]

In addition, polysaccharides including alginate and chitosan have been used in this research, as they are naturally occurring polysaccharides and display numerous characteristics associated with their hemostatic, antioxidant, antitumor, antimicrobial, antifungal, analgesic, and hypocholesterolemic properties.[15,25−30] Moreover, poly(vinyl alcohol) (PVA) was used as a synthetic polymer in this study to facilitate the electrospinning process, besides its various significant and promising characteristics including elevated degrees of swellability, elasticity, a rubberlike structure, bioadhesiveness, noncarcino-

https://dx.doi.org/10.1021/acsomega.9b02832
ACS Omega 2020, 5, 2133−2147

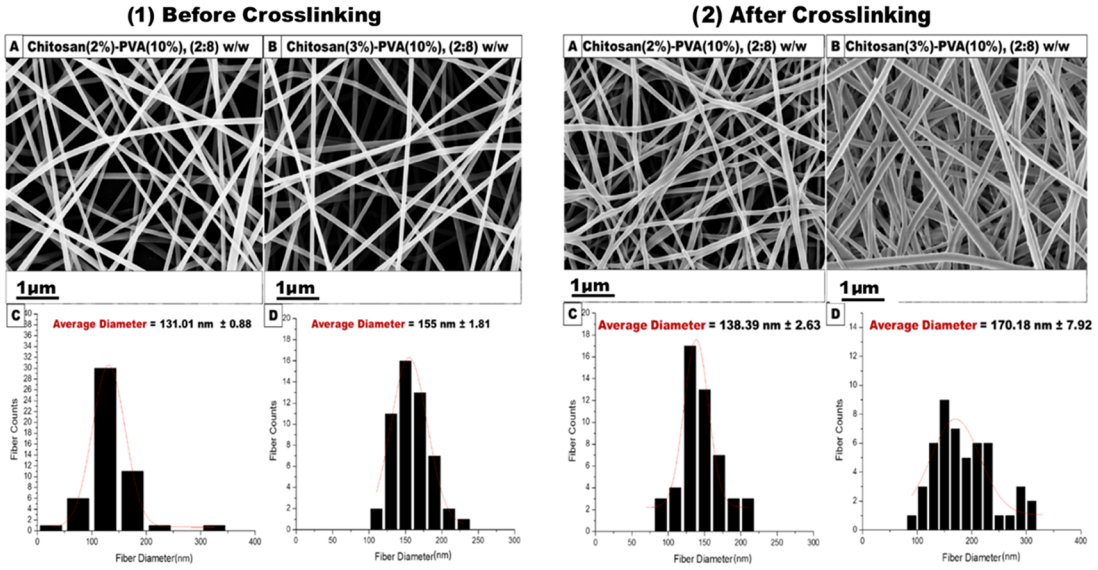

Figure 2. SEM morphological characterization of fabricated nanofibers. (1) Non-cross-linked. (2) Cross-linked at a ratio of 2:8 w/w. (1A) Cs (2%)−PVA (10%) nanofibers with their (1C) corresponding histogram (the average fiber diameter is 131.01 nm; n = 50). (1B) Cs (3%)−PVA (10%) nanofibrous mats along with their (1D) typical histogram (the average fiber diameter is 155 nm; n = 50). (2A) Cs (2%)−PVA (10%) nanofibers with their corresponding (2C) histogram (the average fiber diameter is 138.39 nm; n = 50). (2B) Cs (3%)−PVA (10%) nanofibrous mats along with their (2D) typical histogram (the average fiber diameter is 170.18 nm; n = 50).

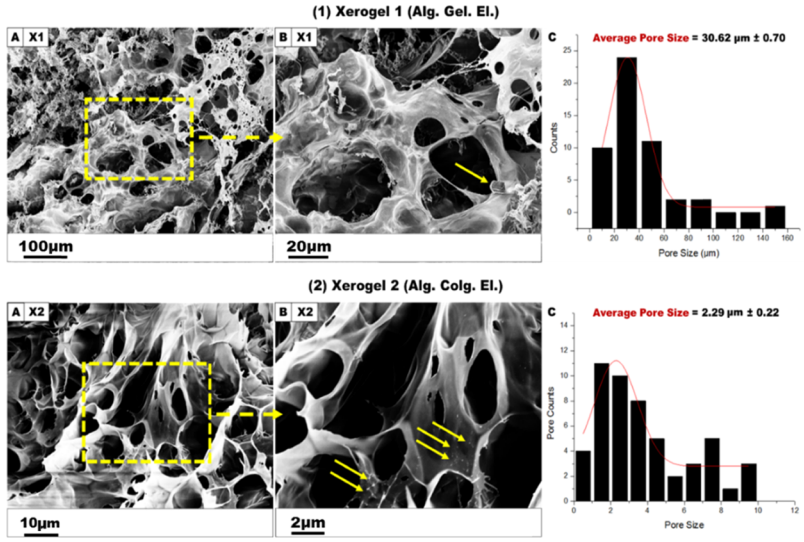

Figure 3. SEM micrographs of cross-linked X1 and X2 xerogel scaffolds. (1A) X1 (Alg. Gel. El.) xerogel heterogeneous structure fabricated in 3% of $CaSO_4$. (1B) X1 SEM photograph at a scale of 20 μm. (1C) Histogram for X1 represents a mean pore size of 30.62 μm (n = 50). (2A) X2 xerogel (Alg. Colg. El) morphology prepared in $CaSO_4$ (3%). (2B) X2 zoom-in SEM micrograph at a 2 μm scale. (2C) Histogram for X2 showing an average pore size of 2.29 μm (n = 50). The yellow arrows indicate the undissolved elastin fibrils.

genicity, and ease of handling properties. In addition, PVA is nontoxic due to its very limited acute oral toxicity.[31−33]

According to the unique properties of the utilized proteins and polysaccharides, a smart combination of these components would result in the rapid healing of burn wounds by providing an imitative environment of normal skin layers that could support cell migration and proliferation.

2. RESULTS AND DISCUSSION

The engineered design of the trilayered asymmetric porous biocomposite scaffold is illustrated in Figure 1. This figure shows the composition of the human skin layers and their thickness, which was found to differ from one site to another and mainly based on the specific function of each layer. It is worth mentioning that several studies reported on the average epidermal thickness to be 0.08−0.1 mm and the average dermal thickness to be 1.5 mm.[34−36] However, the whole engineered scaffold prepared in this study was optimized to a thickness of 0.4 mm to facilitate the uptake capacity of the recipient burnt skin region.[37,38]

2.1. Morphological Characterization of Cs/PVA Nanofibrous Scaffolds. SEM micrographs of non-cross-linked and cross-linked Cs (2%)−PVA (10%) and Cs (3%)−PVA (10%) showed an optimum morphological structure at the nanoscale regarding their random orientation, smooth surface, and bead-free structure, as shown in Figure 2. The average diameter of cross-linked Cs (2%)−PVA (10%) and Cs (3%)−PVA (10%)

https://dx.doi.org/10.1021/acsomega.9b02832
ACS Omega 2020, 5, 2133−2147

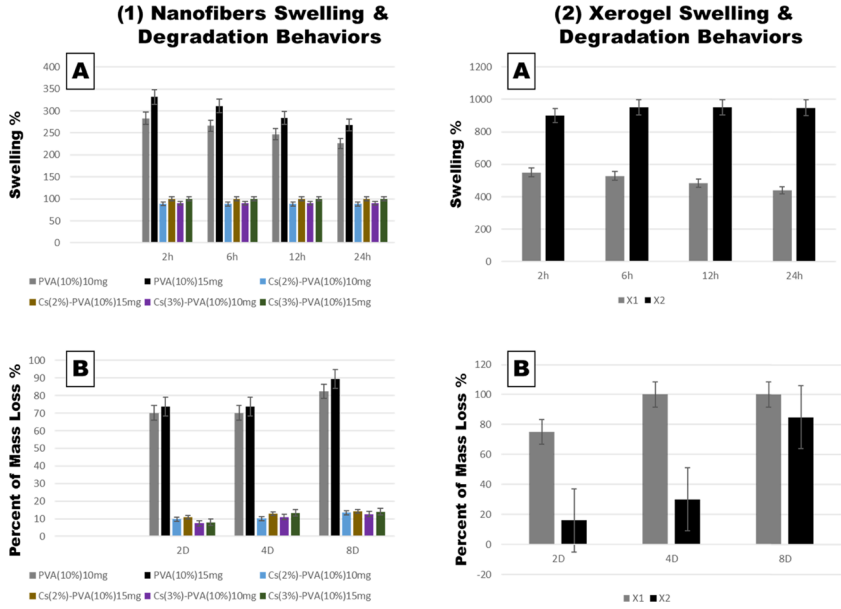

Figure 4. Swelling and degradation capacity of nanofiber and xerogel scaffolds. (1A) Nanofiber swelling behavior. (1B) Nanofiber degradation behavior. All samples were significantly comparable ($P < 0.0001$). (2A) Xerogel swelling capacity ($P < 0.0001$). (2B) Xerogel degradation capacity ($P < 0.01$).

was considerably higher than that of the non-cross-linked ones. The mean diameter of Cs (2%)−PVA (10%) increased from 131.01 to 138.39 nm, and the mean fiber diameter of Cs (3%)−PVA (10%) increased from 155 to 170.18 nm.

This might be attributed to the dispersion of glutaraldehyde molecules into the nanofiber structure homogeneously during the cross-linking process that resulted in shifting the fiber diameter to higher values without forming beads.[39] Furthermore, Cs (3%)−PVA (10%) showed a significant increase in fiber diameter than Cs (2%)−PVA (10%), which was related to the increased Cs concentration that led to the higher viscosity of the electrospun polymeric solution by raising the polymeric chain entanglement and affected the mean size of the fabricated nanofibers. PVA was chosen to achieve a typical nanofibrous scaffold due to its numerous perfect properties such as nontoxicity, biodegradability, biocompatibility, nonionogenic properties, and primary antimicrobial properties for skin tissue regeneration. Since PVA is a nonionogenic polymer, it enhances the charge density of the blended solution and improves the stretch forces of the ejected jet, leading to the formation of smooth, ultrafine, and defect-free nanofibers.[40]

2.2. Morphological Characterization of Xerogel Scaffolds. During the fabrication of the xerogel scaffolds, two similar formulas were used: Alg. (3%). Gel. (6%). El. (11%) (abbreviated to X1) and Alg. (3%). Colg. (0.3%). El. (11%) (abbreviated to X2) at a fixed ratio of (3:7:1.5) (w/w). Elastin was used to provide natural elasticity to the fabricated xerogel scaffolds that could mimic the normal skin elasticity, as elastin represents around 1% of the dermis components and is responsible for the unique elasticity of the normal healthy skin. SEM morphological characteristics of each xerogel sample are presented in Figure 3. For X1, the sample showed quite different morphology compared to that for X2 with a heterogeneous structure and a greater average of pore size (30.62 μm), suggesting that the internal xerogel morphology is affected by its specific composition. However, X2 represented a spherical, macroporous shape with a smooth surface and an average pore size of 2.29 μm.

2.3. Swelling and Degradation Capacity. The swelling and degradation capability of the fabricated cross-linked NFs and xerogels using the phosphate buffer solution (PBS) immersion method are illustrated in Figure 4. For NFs, it has been observed that swelling behavior of cross-linked PVA at 15 mg reached its peak altitude at 332% after 2 h of swelling and then decreased to 268% after 24 h. However, Cs-PVA NF mats showed a considerable decrease in swelling behavior for Cs(2%)−PVA(10%) 15 mg of 99.83%, which slightly increased to 99.89% after 24 h. Moreover, Cs(3%)−PVA(10%) 15 mg exhibited a minor swelling increase of 0.16% after 2 h and then the percentage was lowered to 0.09% after 24 h, indicating the very similar water uptake behavior of Cs at two close concentrations (2 and 3%).

Examined NF scaffolds at a lower weight of 10 mg demonstrated the same swelling behavior but with lower values due to a decrease in polymer contents. The stable manner of water uptake and mass loss of the Cs-PVA NFs mats is due to the chemical interaction between the Cs amine groups and PVA polar hydroxyl groups and the aldehyde groups of glutaraldehyde, which ends up by stable and firmly mechanical features that could control swelling and degradation ability.[41]

Clearly, samples that contained a higher Cs content of 3% expressed a lower degradation rate and slightly higher swelling percentages compared to samples made of 2% Cs. Also, the visibly elevated swellable and degradable manner of single PVA mats was noticed. These two observations could be related to the higher cross-linking density that occurred with the presence of or increased Cs content, due to the more chemical cross-linking between Cs amine groups and GA, which slowed the depolymerization state of NFs containing Cs compared to individual PVA mats.[42]

On the other hand, fabricated xerogels were tested for their swelling and degradation behavior to evaluate their mechanical properties to be further applied to burn wound areas (Figure 4). After 2 h of xerogel immersion in PBS, swelling behavior of X1 xerogel reached up to 650%, while X2 xerogel showed a

https://dx.doi.org/10.1021/acsomega.9b02832
ACS Omega 2020, 5, 2133−2147

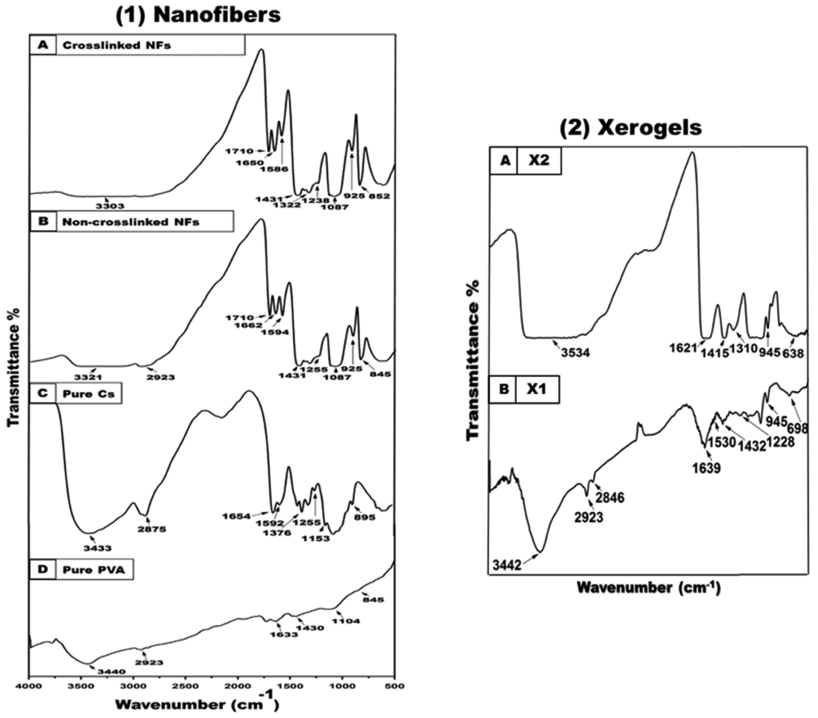

Figure 5. FT-IR spectra of (1D) pure PVA and (1C) pure Cs polymeric powder along with their fabricated composite NFs (1B and 1A). (2) FT-IR absorbed peaks of fabricated xerogels: (2B) X1 xerogel and (2A) X2 xerogel.

greater swelling manner that reached its peak after 6 h (952%) and then roughly decreased to 949% after 24 h. Due to the remarkable capacity, X2 xerogel expressed very low degradation rate after 2 and 4 days (16 and 30%), which then reached up to 85% after 8 days compared to that of X1 xerogel, which was completely softened and fragmented in the stimulated media and totally degraded (100%) after 8 days. This could be explained by the presence of alginate as an elementary material in both xerogels, which contained Ca^{2+} ions. When alginate-based xerogels were immersed in PBS media containing monovalent ions such as Na^{+}, these ions could compete with original Ca^{2+} ions and start to degrade the xerogels over time due to an ion exchange reaction between Ca^{2+} ions and Na^{+} ions.[43] Besides that, it is recognized that collagen, gelatin, and elastin could be readily degraded by proteolytic enzymes.[44]

Surprisingly, collagen is known for its weak mechanical properties;[45,46] however, as mentioned above, X2, which included (Alg. Colg. El.), expressed a low degradation rate, indicating that X2 xerogel is well stabilized by physical cross-linking between functional groups of alginate and collagen.[47] Eventually, low degradation behavior of fabricated NFs and high rate in xerogels made the prepared designed scaffolds ideal in enhancing burn wound healing, as the high degradable rate of xerogels would help their vital components to be easily transported to the burnt area and accelerate the healing process by the formation of new skin tissue. At the same time, lower degradation behavior of prepared NFs is favorable, since the NF layer mats express antibacterial properties, which are crucial in preventing the bacterial invasion to the burnt area. This guarantees the ability of this layer to cover and preserve the burnt area until reaching significant healing.

2.4. Fourier Transform Infrared (FT-IR) Spectroscopy. Functional and chemical groups of the applied pure components and blended nanofibers were investigated using FT-IR spectroscopy. Figure 5 demonstrates the pure Cs and PVA spectrum along with the electrospun non-cross-linked Cs and cross-linked (2%)−PVA (10%) and Cs (3%)−PVA (10%) NFs. Pure Cs absorption peaks of O−H and N−H stretching vibrations were identified at 3433 cm^{-1}. In addition, the C−H stretching was observed at 2875 cm^{-1}. The band at 1654 cm^{-1} is attributed to amide I, while the band at 1592 cm^{-1} is associated with the N−H bending (amide II) and at 1376 cm^{-1} to amide III. The typical weak peak of the amino group was observed at 1255 cm^{-1}, which was linked to the O−H bending vibration. The Cs saccharide and wagging structure were identified at 1153 and 895 cm^{-1}, respectively.[48,49]

Likewise, characteristics peaks of pure PVA were confirmed by FT-IR spectroscopy by determining the O−H stretching vibrations observed at 3440 and 1430 cm^{-1}, which were attributed to the O−H stretching and bending vibration of the PVA hydroxyl group, respectively. The stretching vibration of the asymmetric vibration of the CH_2 group was observed at 2923 cm^{-1} (alkyl groups). Moreover, PVA C═C stretching was found at 1633 cm^{-1}, while C−O stretching was observed at 1104 cm^{-1} and the C−C stretching vibration was observed at 845 cm^{-1} (PVA acetate group residues during its saponification reaction).[42] FT-IR spectra of non-cross-linked and cross-linked Cs (2%)−PVA (10%) and Cs (3%)−PVA (10%) nanofibers were investigated, and the typical characteristic peaks are shown in Figure 5.

FT-IR spectra of the fabricated xerogels showed a shifting of the three characteristic protein peaks of amide I, II, and III to lower wavenumber frequencies upon blending of the different xerogel components, as shown in Figure 5. Moreover, the OH stretching vibration signal becomes broader and is shifted to higher wavenumbers. Additionally, a slight decrease of the absorbed alginate carboxylate groups at 1618 and 1467 cm^{-1} to lower wavenumbers of 1612 and 1461 cm^{-1}, respectively, was observed. Peaks at 1128 cm^{-1} (X1) and 945 cm^{-1} (X2) were related to the CN stretching combined with the NH

https://dx.doi.org/10.1021/acsomega.9b02832
ACS Omega 2020, 5, 2133−2147

Chart 1. Isotherm Linear Plot and Pore Volume Distribution of the Fabricated Xerogels Using BET

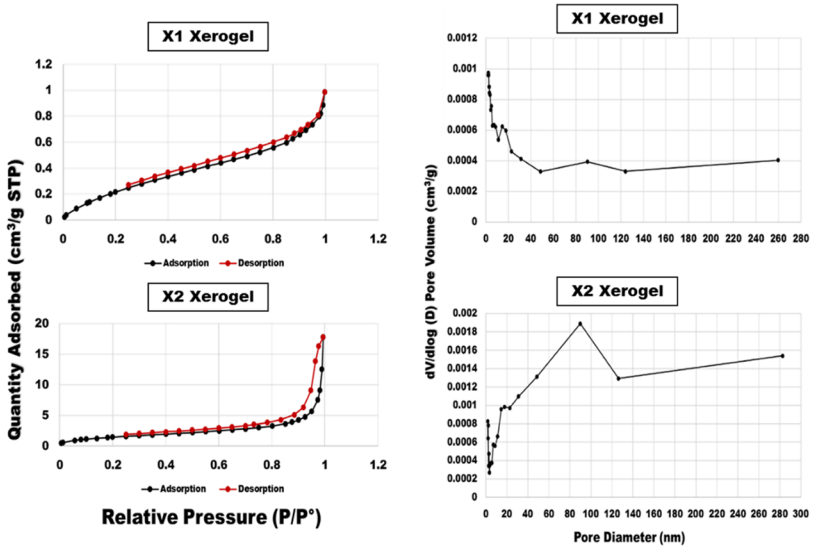

bending upon mixing of the used xerogel components together. Also, the alginate acid peak observed at 720 cm^{-1} was deceased to lower frequencies, while the pyranose ring peak was shifted to 945 cm^{-1}.[50−52]

2.5. Brunauer, Emmett, and Teller (BET) Analysis of Xerogels. The method of Brunauer, Emmett, and Teller (BET) was used to evaluate the pore area and pore size distribution in the fabricated xerogel porous networks. Chart 1 shows the isotherm linear plot and the pore volume distribution of the fabricated xerogels. Apparently, xerogels exhibited two different types of porosities: mesopores (2−50 nm) and macropores (more than 50 nm), according to IUPAC classification.[53] Specifically, X2 xerogel exhibited sharp peaks between 48.42 and 126.23 nm, indicating the presence of a large number of mesopores along with a small quantity of macropores. Meanwhile, X1 displayed a lower quantity of pores identified between 11.13 and 17.68 nm, as well as between 48.44 and 124 nm, demonstrating its mesopores and macropores. Additionally, the total pore surface area (m^2/g) against the pore diameter (nm) of the fabricated xerogels was determined as follows: as shown in Table 1: X1(1.05 m^2/g) and X2 (1.04 m^2/g).

Table 1. Total Pore Volume and Surface Area of the Produced Xerogels

sample name	total pore volume (cm^3/g)	total surface area (m^2/g)
X1	0.0012	1.05
X2	0.0016	1.04

2.6. Mechanical Properties. The tensile strength of fabricated trilayered asymmetric scaffolds was tested using the Tensile Stage TS-1500-lII instrument. Scaffold mats were cut into dog-bone-shaped strips and then held by two-sided grips, and a tensile force was applied. Figure 6 shows the force−displacement curve of the trilayered asymmetric scaffold, which reveals that the fabricated scaffold is flexible. In the beginning, the whole scaffold kept extending up to an applied force of 2.4 newton (N) with a displacement of 3800 μm. The lower xerogel layer (X2) was cracked, while the upper Cs(3%)−PVA(10%) 15 mg kept elongating until reaching the final displacement of 6500 μm.

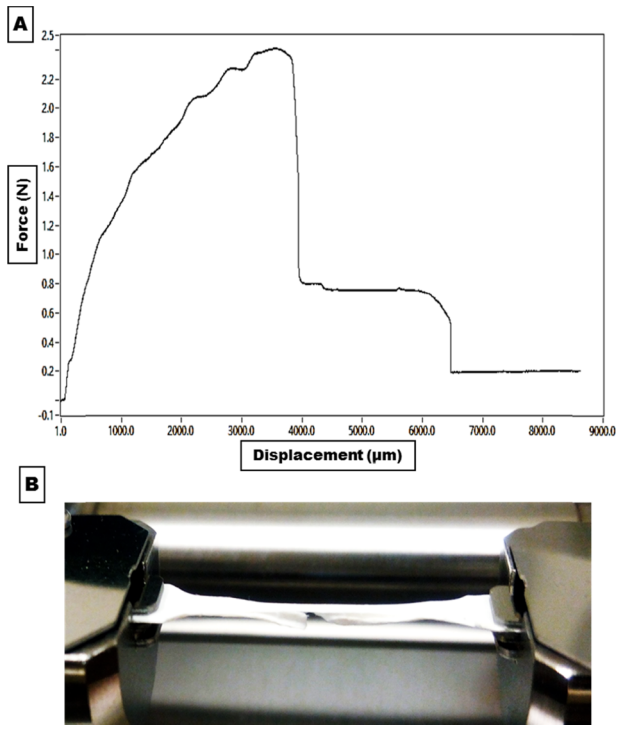

Figure 6. (A) Representative force−displacement curve for the fabricated trilayered asymmetric scaffold. (B) Fabricated scaffold during the tensile mechanical test and the cracked xerogel lower layer.

2.7. Antibacterial Activity of Nanofibrous Scaffolds. Cs antibacterial activity was evaluated at two concentrations (2 and 3%). The fabricated composite nanofibrous scaffolds were tested at two different weights (10 mg and 15 mg). Interestingly, NFs composed of 15 mg of Cs (3%)−PVA (10%) showed a significant activity against both *Staphylococcus aureus* and *Escherichia coli* (log reduction = 3 and 2.70, respectively), while Cs (2%)−PVA (10%) showed lower activity against both tested bacterial strains (log reduction = 2.61 for *S. aureus* and 2.50 for *E. coli*). Meanwhile, the

https://dx.doi.org/10.1021/acsomega.9b02832
ACS Omega 2020, 5, 2133−2147

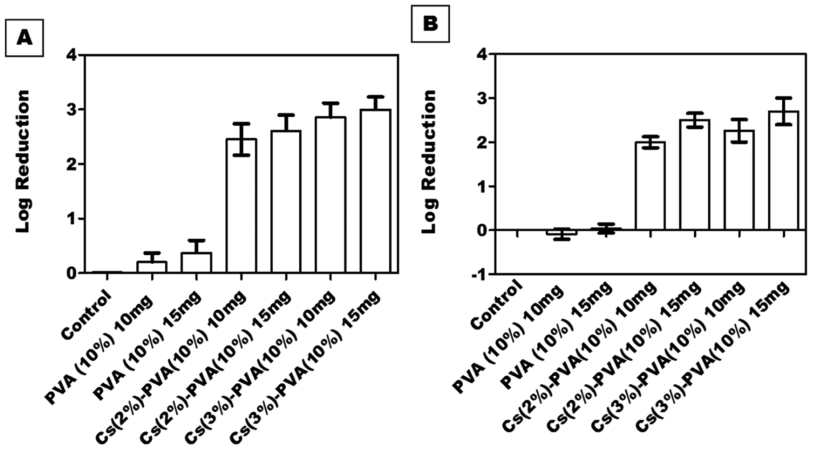

Figure 7. Antibacterial activity of PVA NFs and Cs-PVA NFs against (A) *S. aureus* and (B) *E. coli* at weights of 10 mg and 15 mg. All samples showed a significant decrease in the number of colonies in comparison to control ($P < 0.0001$).

antibacterial effect of both tested samples was slightly decreased when tested at the weight of 10 mg. Cs (3%)−PVA (10%) log reduction value was 2.86 against *S. aureus* and 2.26 against *E. coli*, while Cs (2%)−PVA (10%) expressed a value of 2.45 for *S. aureus* and 2 for *E. coli*, as shown in Figure 7.

Obviously, the number of bacterial colonies decreased with increasing Cs concentration. These results agree with other comparable published results[54] that showed a significant reduction rate in bacterial growth upon increasing the surface area of the utilized Cs nanofibers from 1 to 2.5 cm^2. The reduction rate elevated from 99.93 to 100% in the case of *E. coli* and from 99.14 to 99.98% in the case of *S. aureus*, indicating the greater Cs capability against bacterial colonies at higher concentrations.

The Cs antibacterial activity against both bacterial strains was quite different and had a direct association with the assigned bacterial structure. Generally, Gram-negative bacteria consist of a thin peptidoglycan cell wall with the absence of teichoic acids and the presence of a high-permeability outer membrane (lipopolysaccharides, proteins), which makes them more resistant to antibiotics and more pathogenic. In contrast, Gram-positive bacteria lack the presence of an outer membrane but exhibit a thicker peptidoglycan cell wall with the presence of teichoic acids, which makes them more susceptible to antibiotics.[55] Our fabricated Cs-based nanofibers showed greater bacterial inhibition against *S. aureus* than against *E. coli* since Cs is a polymeric macromolecule and there is an eternal opportunity to pass to the *E. coli* intracellular molecules;[56] instead, it attaches to its negative outer membrane surface (specifically to the anionic components; lipopolysaccharides and proteins) due to its polycationic structure that causes membrane rupture and leakage of the intracellular components.[57]

However, PVA is not widely known with its trivial antibacterial properties, as noticed in this study and the other contemporary study.[58] PVA NFs alone showed more antibacterial activity against *S. aureus* than against *E. coli*, which might be attributed to the expressive degradation capacity of the Gram-negative bacteria than that of Gram-positive bacteria, as most PVA degraders are Gram-negative bacteria.[59] Apparently, PVA at the low tested weight (10 mg) showed a quite increase in *E. coli* bacterial growth (−0.09) than at a higher weight that showed very slight bacterial inhibition (0.04), indicating that *E. coli* has a significant depolymerization effect on lower weights of PVA. Likewise, PVA decreased *S. aureus* growth at 15 mg (0.37) than at 10 mg (0.2), indicating the easy degradation behavior of PVA at low weights and the presence of more alcoholic groups at elevated PVA weights. Table 2 shows the minimum inhibitory concentration (MIC) and the minimum bactericidal concentration (MBC) of the Cs-PVA NFs against both bacterial strains.

Table 2. MIC and MBC of Cs-PVA-Fabricated NFs (mg/mL) Identified by Colony Forming Unit (CFU) against *S. aureus* and *E. coli*

	S. aureus		*E. coli*	
samples	MIC	MBC	MIC	MBC
Cs (2%)−PVA (10%)	10	>15	10	>15
Cs (3%)−PVA (10%)	5	15	10	20

2.8. Cell Culture Assays. *2.8.1. Cytotoxicity Assay.* The proliferation capacity of wild-type (wt) mouse embryonic fibroblast (MEF) on the prepared electrospun NFs and fabricated xerogels was determined by the 3-[4,5-dimethyl-2-thiazolyl]-2,5-diphenyl-2*H*-tetrazolium bromide (MTT) assay. The yellow tetrazolium MTT molecule could be reduced by the active metabolic cells upon the action of dehydrogenase enzymes and secrete the intracellular purple formazan into the examined extraction media. In this study, the developed change in the medium color was determined by spectrophotometric means after 24 and 48 h for all tested samples.[60] PVA nanofibrous and alginate xerogel mats were used as a positive control for the tested nanofibrous and xerogel samples, respectively, while seeded MEFs in Dulbecco's Modified Eagle's Medium (DMEM) media without fetal bovine serum (FBS) were treated as a negative control and expressed as 100% cell viability.

2.8.1.1. Nanofibrous Scaffolds. MEF optical density (OD) on all tested NF samples increased during both assigned interval times, i.e., 24 and 48 h. This indicates that the wt MEF cells were metabolically active in the presence of the fabricated NF and xerogel scaffolds. For NF scaffolds, the difference in cell proliferation was observed between 24 and 48 h. The percentage increase in the proliferation rate from 24 to 48 h was observed in both Cs(2%)−PVA (10%) and Cs(3%)−PVA(10%) NF samples, unlike PVA NFs alone, which showed

https://dx.doi.org/10.1021/acsomega.9b02832
ACS Omega 2020, 5, 2133−2147

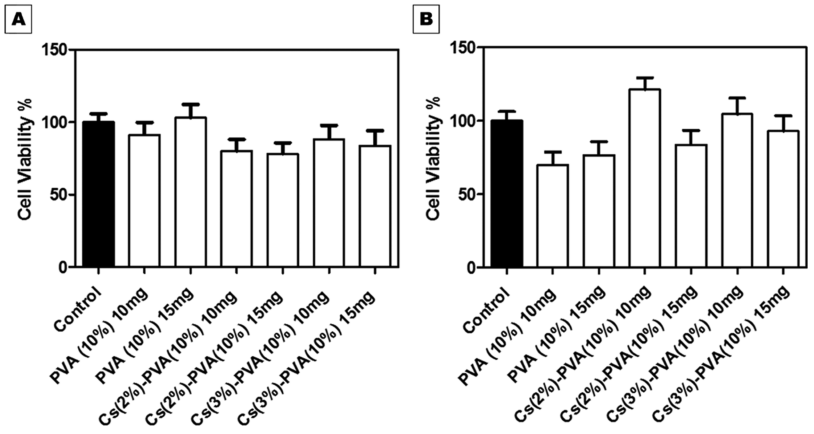

Figure 8. In vitro Cs-PVA nanofibrous mat cytotoxicity tested on seeded wt MEF cells at (A) 24 h and (B) 48 h. The spectrophotometric OD of 570 nm was used. All tested NFs samples expressed significant cell viability ($P < 0.0001$).

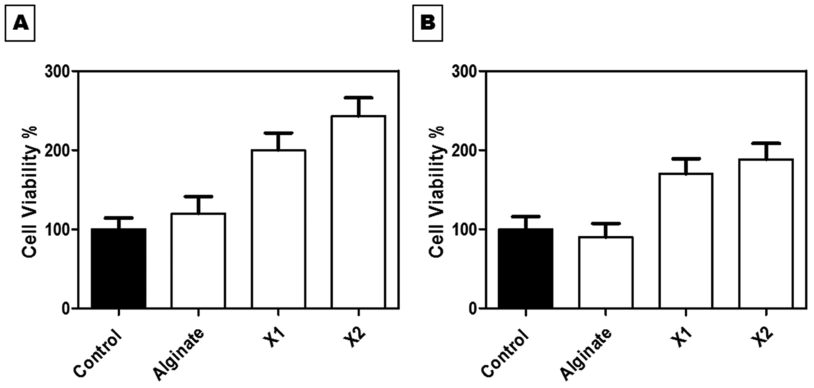

Figure 9. MEF cell viability percentage against the fabricated xerogels: alginate, X1, and X2 (A) at 24 h and (B) at 48 h. All samples showed a significant increase in cell viability ($P < 0.0001$).

less cell viability in 48 h. This might be attributed to the slower degradation rate of Cs-PVA NFs mats compared to that of PVA NFs mats alone, as previously mentioned in the biodegradability study. All examined NF samples ensured significantly their biocompatibility and nontoxicity ($P < 0.0001$) toward MEF by demonstrating the percentage of cell viability above 50% with closer or higher proliferation values compared to those of the control, as shown in Figure 8.

2.8.1.2. Xerogel Scaffolds. Fabricated xerogel scaffolds demonstrated remarkable and great cell viability rates when incubated for 24 and 48 h. All examined samples showed a significant elevation in cell reproduction rate ($P < 0.0001$) compared to the untreated control samples, as shown in Figure 9. In the first 24 h, the MEF cell viability rate increased dramatically and reached 243% in the case of X2 and decreased to (200%) when tested with X1, in contrast to that of the control (100%). After 48 h, the metabolic activity of live cells noticeably decreased to 106 and 188.4% for X1 and X2, respectively. These results were in conformity with the biodegradable study (Figure 4), which revealed the highly degradable rate of the xerogel components within 8 days. This could signify the correlation between the biodegradability of the produced xerogels and cell viability.

As anticipated, the percentage of cell viability was higher in the presence of collagen and elastin together, as shown in X2 compared to the control sample. It is widely known that collagen plays a definitive and critical role in managing cell biological functions and behaviors, as it could regulate cell proliferation, adhesion, migration, and differentiation. This is attributed to the existence of three unique amino acids in collagen that are arranged together in a specific configuration and direct the proliferation of targeted cells. Most importantly, the used collagen in this study is type I, which constitutes around 80−85% of fibroblasts; thus, there might be some cell signaling between the cultured mouse fibroblast cells and the X2 xerogel condition medium, which is rich in collagen.[61−65]

Gelatin differs from collagen in its configuration shape that changes the recognition sites for cell binding, as it expresses a less ordered macromolecular structure than collagen. Both molecules own E (glutamate) or D (aspartate) residues necessary for cell attachment, but collagen varies from gelatin by having the attracted triple helical GxOGER sequences (G is glycine; O is hydroxyproline; R is arginine; and x is hydrophobic, represented by phenylalanine, F). Meanwhile, gelatin substitutes this highly affinitive molecule by a linear cell adhesive ligand, RGD. Subsequently, this alters the typical order of cell binding sites, leading to variation in cell behavior in the presence of each molecule separately. This explains how X2 xerogel showed high cell viability (243%) compared to X1 (141.14%) that contained gelatin along with elastin and alginate.[66]

Similarly, as mentioned above, elastin includes about 3−9 short repeated amino acid sequences that regulate it to its determined arrangement. One study has proven that GAGs could bind to the bovine tropoelastin C-terminal region, while another study has reported the tropoelastin cell interactive site

https://dx.doi.org/10.1021/acsomega.9b02832
ACS Omega 2020, 5, 2133−2147

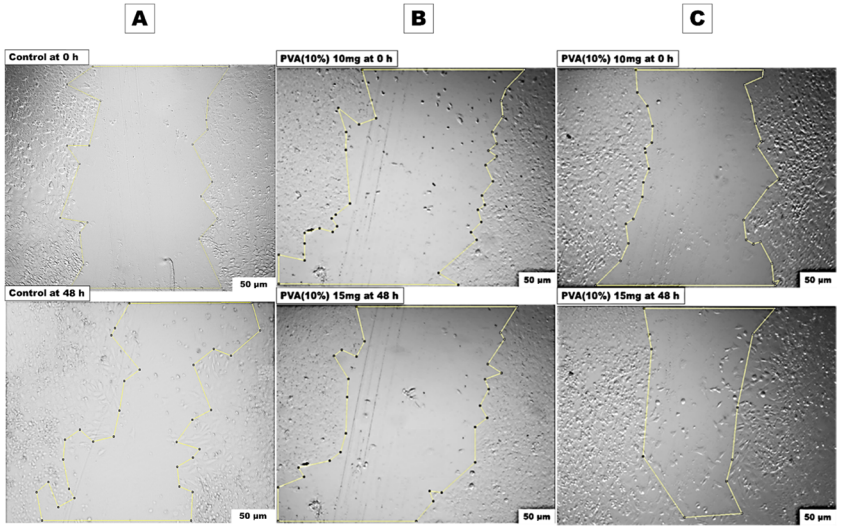

Figure 10. In vitro scratch assay at two interval times (0 h and 48 h) of (A) negative control MEFs in DMEM media. (B) PVA (10%) in 10 mg/mL condition media. (C) PVA (10%) in 15 mg/mL condition media.

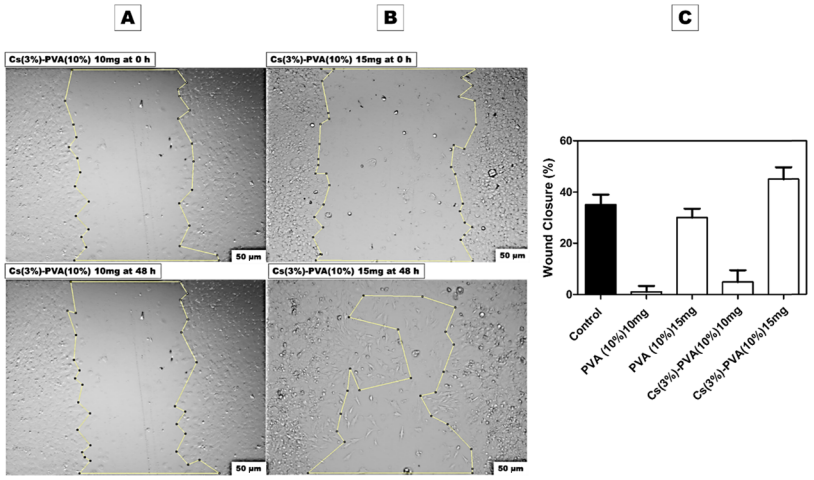

Figure 11. In vitro scratch assay at 0 and 48 h against (A) Cs(3%)−PVA(10%) 10 mg/mL condition media and (B) Cs(3%)−PVA(10%)15 mg/mL condition media. (C) Wound closure percentage of all tested nanofibers samples after 48 h using Image J.

to be situated in the central domain 17−18 domain region, more specifically, in the 18-sequence domain. It has been detected that GAGs and integrins, which are present on the cell surface, can identify this sequence distinctly from the total tropoelastin molecule. Since elastin represents around 1−2% of the total dermis layer, the integration of elastin with collagen or gelatin enhances the cell viability, as shown in X1 and X2 xerogels.[67]

2.8.2. In Vitro Scratch Assay. The NFs and xerogels along with their individual condition medium were evaluated for their capability of enhancing MEF cell migration in a 96-well plate, which is a crucial assessment in this study to comprehensively determine the samples that could significantly close the wounded area rapidly.

2.8.2.1. Nanofibrous Scaffolds. Figure 9 shows the artificially induced wt MEF gap for the negative control sample at 0 h, which showed a significant cell migration of 35% after 48 h. In contrast, Figure 11 shows Cs(3%)−PVA(10%) at 15 mg with an expressive cell migration of 45.04%, making it highly biocompatible and efficient in wound closure compared to both negative and positive control samples.

The positive control PVA (10%) NFs are shown in Figure 10 at two examined weights of 10 mg and 15 mg. Surprisingly, PVA mats at the weight of 10 mg demonstrated very negligible cell migration (1%), while at a higher PVA weight (15 mg), the cell migration elevated up to 30.05%, which was very close to the percentage of the control negative sample, demonstrating the nontoxicity of PVA.[68−70] This may be attributed to the low weight of 10 mg used at the beginning, as PVA is reported to lack the presence of cell binding sites that encourage the cell migration, while at the higher PVA weights, it improved the cell migration capacity. These results are in agreement with the results of the cytotoxicity study that showed higher cell viability at 15 mg PVA than at 10 mg PVA (Figure 7).

Similarly, the same results were observed with Cs (3%)−PVA (10%) 10 mg that expressed a wound closure percentage of 4.86% compared to the Cs(3%)−PVA(10%) 15 mg sample that expressed an elevated wound closure percentage of 45.04%, as shown in Figure 11. Despite the naturally found polysaccharide properties of Cs and its mimicking structure for the ECM GAGs along with its numerous benefits such as biodegradability, antibacterial properties, and biocompatibility,

https://dx.doi.org/10.1021/acsomega.9b02832
ACS Omega 2020, 5, 2133−2147

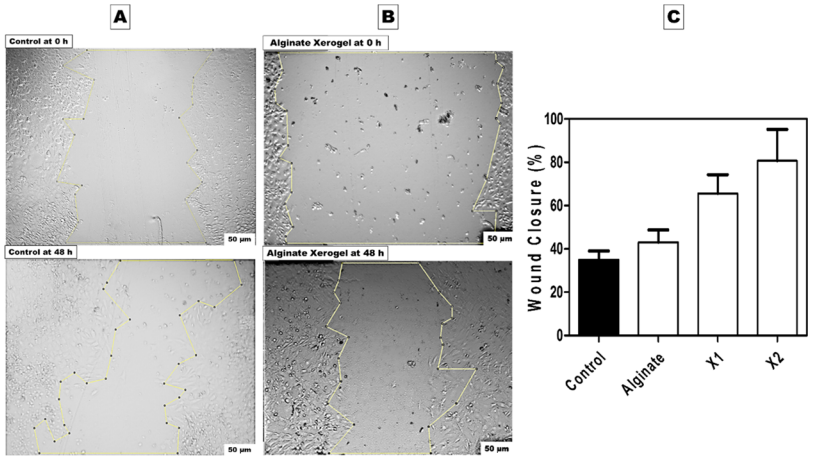

Figure 12. In vitro scratch assay for fabricated xerogels at 0 and 48 h. (A) Negative control MEFs in conventional DMEM media. (B) Positive alginate xerogel control condition media on seeded MEFs. (C) Column graph of in vitro wound healing assay in the presence of all fabricated xerogels condition media after 48 h.

the Cs degree of deacetylation in some cases could affect the cell migration, as observed during this study. A comparable research study has observed a rounded shape of adult human bone marrow-derived stem cells when implanted in pure Cs. DNA investigation of this cell line revealed a lower DNA content of the examined cells over 3 weeks of up to 50%, indicating the occurrence of cell death.[65] Other study produced Cs gels embedded with rat-muscle-derived stem cells in β-GP, which demonstrated a similar round shape when cultured for 4 weeks in vitro and in vivo.[62]

In our study, the NF samples did not show rounded cell morphology and instead expressed low migration rates in the case of Cs(3%)−PVA(10%) NFs at low weight (10 mg). This could mainly relate to the high Cs deacetylation degree (89.9%) that could negatively affect the cultured cell behavior. More clearly, wt MEF cells were migrated in the presence of a higher sample weight (15 mg) rather than a lower weight (10 mg), indicating that the cells were able to migrate just at the elevated content of PVA-Cs-combined NFs mats since Cs and PVA are polymers that do not require specific ligands for cell affinity.

2.8.2.2. Xerogel Scaffolds. Figures 12 and 13 show the induced artificial wound at 0 and 24 h for the produced X1 and X2, which revealed accelerating wound healing of 65.63 and 80.74% for each one, respectively. This data is in agreement with the MTT assay results, which identified the highest cell viability in X2. According to the above-mentioned observation, the addition of gelatin to collagen significantly decreased the cell viability and cell migration. Following that, the less specificity of the gelatin RGD ligand led to lower cell growth and migration compared to collagen that exhibited higher and more specific binding sites, which aided in targeting cell growth.[66,71] Moreover, Figure 13 shows that numerous mitotic cells were attached to the established monolayer sheet and appeared as rounded cells, indicating the healthy state of the cultured wt MEF cells in both X1 and X2 samples. X2 sample after 48 h shows migrated cells expressing a spindle-shaped morphology, which resembled collagen fibers, indicating a cellular reaction between the cells and collagen matrix. These findings are pointing to cellular interaction events between collagen-specific integrins and cell migration that might need further investigation.

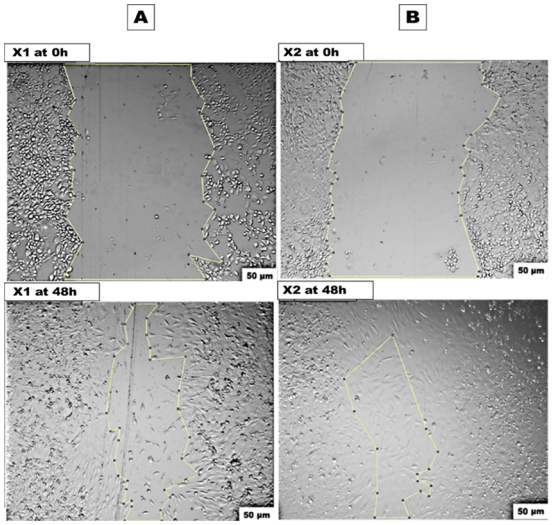

Figure 13. In vitro scratch assay of fabricated xerogel condition media at 0 and 48 h. (A) X1 and (B) X2.

2.9. Migration Capability of MEF in the Presence of the Designed Asymmetrical Trilayered Scaffold. The layers of the typical trilayered scaffold were chosen based on the efficacy of the characterized nanofibrous and xerogel samples, separately. At this stage, Cs(3%)−PVA(10%) 15 mg NF mats and the X2 mat-containing sample (Alg. Colg. EL) were selected to act as upper and lower layers, consequently. These two asymmetrical layers in morphology and function were fixed together using fibrin glue, ending up with three different structural layers. Collagen, gelatin, elastin, and fibrin glue possess cell-binding-specific ligands that could interact and direct cell migration. This was observed for the wt MEF cell migration capacity, which improved when tested against the asymmetric trilayered scaffold compared to the individual tested scaffold layers. To the best of our knowledge, there is no reported study on the influence of fibrin glue on wt MEF cells regarding their growth and migration; instead, multiple studies have reported its effect on other examined cell lines including bone marrow mononuclear cells, mesenchymal stem cells, vascular smooth muscle cells, and adipose-derived stem cells.[72−74] Apparently, the migrated cell morphology in Figure

https://dx.doi.org/10.1021/acsomega.9b02832
ACS Omega 2020, 5, 2133−2147

14 after 48 h represents the healthy spindle-extended morphology of the newly migrated cells, which covered the

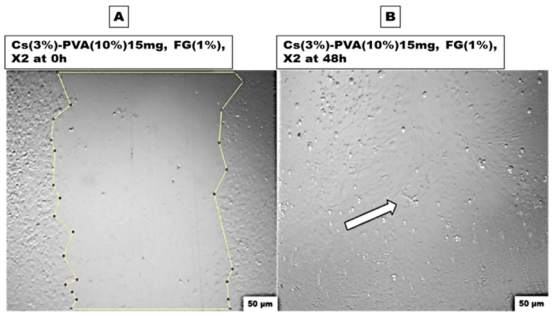

Figure 14. Evaluation of the finally designed scaffold capacity using the in vitro wound healing assay: (A) at 0 h and (B) after 48 h. The white arrow indicates complete healing.

artificial wounded gap without experiencing cell stress or death according to their healthy morphology.

3. CONCLUSIONS

In this study, we successfully developed an innovative, highly biocompatible, and biodegradable asymmetric trilayered scaffold for skin regeneration. The scaffold expressed unique antibacterial properties with log reduction values of 3 and 2.70 in the case of 15 mg Cs (3%)−PVA (10%) (as an upper layer) against both *S. aureus* and *E. coli*, respectively. Stable and high swelling behavior over time was observed for the upper layer 15 mg Cs(3%)−PVA(10%) (99.98%), with a degradable rate of 14% compared to PVA(10%) and Cs(2%)−PVA(10%) tested samples. A similar observation was noticed in the case of the X2 xerogel sample, which showed swelling behavior of up to 949% and a degradation rate of 85% after 24 h compared to the X1 sample, which presented 441 and 100%, respectively. This optimum swelling capability is essential in absorbing wound exudates, especially in the first 24 h, besides the great biodegradability over time of the sample. Furthermore, NF average diameter and xerogel pore size distribution were determined using SEM and BET. The upper Cs(3%)−PVA (10%) showed an NF average diameter of 170.18 nm, while X2 expressed a pore size distribution in the range of 48.42−126.23 nm with a pore volume of 0.00188 cm^3/g. The findings of this study showed the capability of the fabricated polymer-based ECM artificial composite in favoring and supporting fibroblast migration and proliferation without significant cytotoxicity. This was demonstrated in vitro when the MEF cell migration capacity leveled up to 95% compared to the control sample, which showed only 35% of cell migration after 48 h. Since the majority of the used components resemble or naturally exist in the skin ECM, they tremendously assist and reinforce the induced in vitro artificial wound healing. The reported results are inspiring in the domain of skin tissue engineering, making the created asymmetric composite ideal and superior for promoting skin regeneration after chronic skin burns.

4. MATERIALS AND METHODS

4.1. Materials. Chitosan (Cs) of low molecular weight (89.9% degree of dealkylation) was purchased from Primex ehf, Chitoclear, Iceland. Glacial acetic acid (CH_3COOH) was purchased from Thermo Fisher Scientific Inc. Sodium alginate (Protanal LF 10/60 NF) was supplied by FMC BioPolymer, Philadelphia. Gelatin was purchased from Honeywell Fluka Research Chemicals, Germany. MTT reagent (3-[4,5-dimethyl-2-thiazolyl]-2,5-diphenyl-2H-tetrazolium bromide) and dimethyl sulfoxide (DMSO) were purchased from Serva Electrophoresis, Heidelberg, Germany. Phosphate buffer solution (PBS) was obtained from Lonza, Switzerland. Fibrinogen type I-S (65−85% protein) from bovine plasma, thrombin from bovine plasma (40−60% protein, 40−300 NIH units/mg protein), elastin from bovine neck ligament, collagen type I solution from bovine skin, Dulbecco's modified Eagle's medium (DMEM), poly(vinyl alcohol) (PVA) (M_w = 125 000 kDa), calcium sulfate dihydrate salt ($CaSO_4.\ 2H_2O$), and glutaraldehyde solution (25%) were purchased from Sigma Aldrich, Germany. *E. coli* (ATCC 8739) and *S. aureus* (ATCC 6538) were purchased from the American Type Culture Collection.

4.2. Preparation of Cs/PVA Nanofibrous Scaffolds. Two different concentrations of Cs were prepared (2% and 3% wt) in 1% glacial acetic acid. PVA was prepared at concentrations of 9 and 10% wt in highly purified hot distilled water (D.W; 80 °C). Cs-PVA blends were prepared in two different weight ratios (1:9 and 2:8). To obtain a well-blended polymeric mixture, the Cs-PVA solutions were left to mix for 4 h on a continued stirrer.

The resulting beadless nanofiber mesh was chosen to be used within the asymmetric scaffold structure and for further characterization tests. The electrospinning process was started by inducing the prepared blends into a 10 mL plastic syringe placed in a syringe pump and connected to a silicone tube, which allows solutions to flow with a flow rate of 0.8 mL/h through the stainless steel needle of the syringe. The electrical voltage was fixed to 18 kV applied to the needle tip, and the tip-to-collector distance was settled at 12 cm. The produced nanofiber meshes were collected on a flat stationary copper plate collector covered with an aluminum foil. The resultant nanofibers were cross-linked in a sealed desiccator using 25% of aqueous glutaraldehyde solution and left for 12 h and then dried in a vacuum oven for 2 h at a temperature of 60 °C to dispose of glutaraldehyde residual remnants.[28]

4.3. Xerogel Synthesis. Elastin (El.) powder with a concentration of 11% was dissolved in DMSO and added to collagen (Colg., 0.3%) and alginate (Alg., 3%) (to develop X1 xerogel) or to gelatin (6%) and alginate (3%) (to develop X2 xerogel). The (Alg. Gel. El., X1) solution was fixed to the weight ratio of 3:7:1.5, while the (Alg. Colg. El., X2) solution was fixed to the ratio of 7:1.5:1.5. Alginate polymeric solution was prepared at a concentration of 3% to develop single alginate xerogel mats. The X1 and X2 xerogel scaffolds were synthesized using the internal gelation method and freeze-drying technique. All polymeric solutions were mixed overnight to ensure perfect homogenization at 37 °C. The obtained mixtures were further poured in 83 mm glass Petri dishes and then cross-linked in 3% $CaSO_4.2H_2O$ at room temperature to allow gelation for 1 h, followed by lyophilization for 12 h to produce the dry form of a hydrogel, which is the xerogel. The fabricated samples were kept at room temperature for further use.

4.4. Scaffold Characterization. Xerogel scaffolds were examined for their porosity, pore surface area distribution, and pore diameter dispersion using a mercury intrusion porosimeter under elevated pressure from 100 kPa to 207 MPa. Washburn mathematical eq 1 was used to determine the mean pore size for each sample

https://dx.doi.org/10.1021/acsomega.9b02832
ACS Omega 2020, 5, 2133−2147

$$D = (-4\gamma \cos\theta)/P \quad (1)$$

where (P) is referring to the applied pressure, (D) to the pore diameter, (γ) to the mercury surface tension (484 mN/m), and (θ) is the mercury pore wall contact angle measured as 141.31 °C.

Fabricated NF and xerogel scaffolds were tested for their swelling and degradation behavior in a stimulated PBS medium (37 °C) at certain time intervals (2, 6, 12, and 24 h). The scaffold weight was measured before and after immersion in PBS swelling medium to calculate the swelling ratio as per eq 2. The process was performed in triplicates for each investigated sample and continued until reaching a steady weight, and the measurements were demonstrated as ± mean standard deviation.

$$\text{degree of swelling (\% of PBS up take)} = M_a - M_b/M_b \times 100 \quad (2)$$

where M_b represents the weight of the samples before immersion in the swelling buffer and M_a indicates the weight of the samples after immersion for specific time intervals (t).

The scaffold degradation rate (mass loss %) was evaluated by drying the samples at room temperature under vacuum until reaching a fixed weight and re-weighting at 2, 4, and 8 days, according to eq 3

$$\text{mass loss (\%)} = M_b - M_d/M_b \times 100 \quad (3)$$

where M_b represents the weight of the samples before immersion in PBS buffer and M_d refers to the weight of the samples after complete dehydration (%).

4.5. Evaluation of in Vitro Antibacterial Activity. Gram-negative bacteria (*Escherichia coli*) and Gram-positive bacteria (*Staphylococcus aureus*) were used to assess the antibacterial capacity of the created nanofiber scaffolds. The nanofiber mats (Cs 2%−PVA10%, Cs 3%−PVA10%, and PVA10%) were investigated at fixed concentrations (10 mg and 15 mg/mL) of each sample using the broth dilution method. The bacterial inoculum was prepared by preculturing the Gram-negative and -positive bacteria in Difco nutrient broth (NB) at a temperature of 37 °C, which then was left overnight on a rotating shaker at 225 rpm. The optical density (OD600) of the bacterial overnight culture was standardized spectrophotometrically to be 0.1 × 108 CFU/mL. Afterward, the test tubes including the examined nanofiber samples were incubated overnight (14−18 h) at 37 °C on a rotating shaker at 225 rpm. Following that, a stepwise dilution was done for each overnight cultured sample until reaching a dilution of 10^{-5} for *E. coli* and 10^{-7} for *S. aureus* using nutrient broth media. Then, the diluted samples were plated on Difco nutrient agar plates and incubated overnight at 37 °C.

CFU per mL of the overnight culture was calculated according to eq 4[75] as follows

$$N = C \times 10/10^{-D} \quad (4)$$

where N = CFU/mL, C = the number of colonies per plate, and D = the number of the 1:10 dilution.

The MIC of the tested samples were first identified manually by visual observation at a dilution factor of 10^{-5} for *E. coli* and 10^{-7} for *S. aureus* when diluted in sterile Eppendorf tubes. This observation was then confirmed by stepwise dilution of each sample using NB media in a sterile 96-well microtiter plate. Then, the MIC was read using the microplate reader 65 (SPECTROstar Nano, BMG LABTECH, Germany) after overnight incubation of the culture at 37 °C.[75]

Moreover, the MBC of the tested NF samples was evaluated visibly by subculturing the broths used for MIC determination onto fresh agar plates and incubating overnight at 37 °C. The MBC was determined by visual observation of the lowest broth dilution that was successful in restraining the growth of each examined *E. coli* and *S. aureus* bacterial strains separately on the agar plates.[76]

The test was done in triplicates for each tested sample, and the conventional plate count was used to identify the number of viable bacterial colonies.

4.6. Cell Culture Assay. Wild-type (wt) mouse embryonic fibroblasts (MEFs) were cultured as a monolayer in DMEM media complemented with 4500 mg/L glucose, L-glutamine, sodium pyruvate, sodium bicarbonate, 10% fetal bovine serum (FBS), and 100 μg/mL streptomycin. wt MEF cells were passaged three times every week in 75 cm^2 tissue culture flasks and incubated in a 5% CO_2 incubator (Heracell incubator, Thermo Scientific) at 37 °C. Trypsin (0.25%) containing 0.1% ethylenediaminetetraacetic acid was used in cell detachment before passaging or before the specified assays. Trypan blue was used in cell counting using a hemocytometer.

All examined scaffold specimen mats were sterilized for 1 h (for each side) using UV radiation. Thereafter, all samples were neutralized using PBS (pH 7.4) for 30 min to remove any acidic or glutaraldehyde traces. Following that, submerging in DMEM with different weight concentrations (10 mg and 15 mg/mL for nanofiber mats and 25 mg/mL for hydrogel mats) and incubation overnight at 37 °C were done to produce condition media with various examined concentrations. Seeded wt MEF cells with conventional DMEM media were used as a negative control, while cultured wt MEF cells with PVA nanofibrous or alginate xerogel mat condition media were used as a positive control for nanofiber mats and xerogels, respectively.

The samples were investigated in triplicates, and the average of results was plotted as mean ± standard error.

4.6.1. Indirect Cytotoxicity Assay. Fabricated scaffolds were tested for their cytotoxicity against wt MEF cell lines according to the ISO10993-5 standard-based procedure. wt MEF cells were cultured in a 96-well plate at a density of 3000 cells/well to reach semiconfluency after 24 h, and then the medium was exchanged with the different concentrations of the incubated condition media and reincubated once for 24 h and once for 48 h. After treatment, the condition solutions were replaced by 100 μL of 1 mg/mL MTT reagent for each well and left for 4 h. Following that, the cells were washed with PBS twice after removing the MTT medium and 100 μL/well of a 100% DMSO was added to dissolve the formazan crystals formed in living cells. Cell viability was identified using the microplate reader 65 (SPECTROstar Nano, BMG LABTECH, Germany) at an absorbance (ABS) of 570 nm. The viability of negative control samples was recognized as 100% and calculated according to eq 5 as follows

$$\text{cell viability rate} = \text{sample ABS/control ABS} \times 100 \quad (5)$$

4.6.2. In Vitro Two-Dimensional Wound Healing Assay (Mechanical Wounding). The scratch assay was used to evaluate the capacity of the fabricated nanofibrous and xerogel scaffolds in enhancing cell migration. wt MEF cells were seeded at 5000 cells/well in a 96-well plate to reach confluency after 24 h. A straight line was produced in the middle of each

https://dx.doi.org/10.1021/acsomega.9b02832
ACS Omega 2020, 5, 2133−2147

sample well to create a scratch using the p10 pipette tip. The wound was induced before replacing the DMEM conventional media with the prepared condition ones and washed with PBS two times to remove any cell debris and soften the wound edges and then 100 μL/well of each sample condition medium was added. The closure of the different created wounds was examined periodically at specific time intervals (0, 24, and 48 h) using the Olympus IX70 fluorescence microscope. Image J analysis software was used to assess the wound closure behavior of each induced scratch beginning from $t = 0$ to the last interval point, and the wound recovery (%) was calculated according to eq 6

$$\text{wound recovery } (\%) = XT_0 - XT_x/XT_0 \times 100 \quad (6)$$

where XT_0 refers to induced wound area at $t = 0$ and XT_x is the wound area at a specific time interval point.

AUTHOR INFORMATION

Corresponding Author

Wael Mamdouh − *Department of Chemistry, School of Sciences and Engineering, The American University in Cairo (AUC), New Cairo 11835, Egypt;* orcid.org/0000-0003-0642-1992; Phone: +202 2615 2555; Email: wael_mamdouh@aucegypt.edu; Fax: +202 2797 4951

Author

Fatma Elshishiny − *Department of Chemistry, School of Sciences and Engineering, The American University in Cairo (AUC), New Cairo 11835, Egypt*

Complete contact information is available at: https://pubs.acs.org/10.1021/acsomega.9b02832

Author Contributions

The manuscript was written through the contributions of all authors (F.E. and W.M.). All authors approved the final version of the manuscript.

Funding

The project was funded through faculty and student research grants provided by the American University in Cairo.

Notes

The authors declare no competing financial interest.

ACKNOWLEDGMENTS

The authors gratefully acknowledge Dr. Andreas Kakarougkas at the Biology department, The American University in Cairo, for providing a viable stock of the MEF living cells and the research assistant Salma El-Shafei for providing full tissue culture training.

ABBREVIATIONS

MTT, 3-[4,5-dimethyl-2-thiazolyl]-2,5-diphenyl-2*H*-tetrazolium bromide; NB, nutrient broth; NFs, nanofibers; MEF, mouse embryonic fibroblast

REFERENCES

(1) Burns. https://www.who.int/news-room/fact-sheets/detail/burns (accessed May 3, 2019).

(2) CDC, Burns. https://www.cdc.gov/masstrauma/factsheets/public/burns.pdf (accessed May 16, 2019).

(3) Hettiaratchy, S.; Dziewulski, P. Pathophysiology and Types of Burns. *BMJ* **2004**, *328*, 1427−1429.

(4) Burns. https://www.nigms.nih.gov/education/pages/factsheet_burns.aspx (accessed Nov 29, 2018).

(5) Jun, I.; Han, H.-S.; Edwards, J.; Jeon, H. Electrospun Fibrous Scaffolds for Tissue Engineering: Viewpoints on Architecture and Fabrication. *Int. J. Mol. Sci.* **2018**, *19*, No. 745.

(6) Foncerrada, G.; Capek, K. D.; Herndon, D. N.; Lee, J. O.; Sirvent, R. Z.; Finnerty, C. C. The State of the Art on Burn Wound Healing. *J. Avid Sci.* **2017**, 4−52.

(7) Abbasipour, M.; Mirjalili, M.; Khajavi, R.; Majidi, M. M. Coated cotton gauze with Ag/ZnO/chitosan nanocomposite as a modern wound dressing. *J. Eng. Fibers Fabr.* **2014**, *9*, No. 155892.

(8) Thornton, J. F.; Gosman, A. A. Skin Grafts and Skin Substitutes. In *Selected Readings in Plastic Surgery*; Baylor University Medical Center: Dallas, 2004; Vol. *10*, pp 1−24.

(9) Meleshina, A. V.; Bystrova, A. S.; Rogovaya, O. S.; Vorotelyak, E. A.; Vasiliev, A. V.; Zagaynova, E. V. Skin Tissue-Engineering Constructs and Stem Cells Application for the Skin Equivalents Creation (Review). *Sovrem. Tehnol. Med.* **2017**, *9*, No. 198.

(10) Rashaan, Z. M.; Krijnen, P.; Allema, J. H.; Vloemans, A. F.; Schipper, I. B.; Breederveld, R. S. Usability and Effectiveness of Suprathel in Partial Thickness Burns in Children. *Eur. J. Trauma Emerg. Surg.* **2017**, *43*, 549−556.

(11) Calabrese, G.; Forte, S.; Gulino, R.; Cefalì, F.; Figallo, E.; Salvatorelli, L.; Maniscalchi, E. T.; Angelico, G.; Parenti, R.; Gulisano, M.; et al. Combination of Collagen-Based Scaffold and Bioactive Factors Induces Adipose-Derived Mesenchymal Stem Cells Chondrogenic Differentiation In Vitro. *Front. Physiol.* **2017**, *8*, No. 50.

(12) Gaspar, A.; Moldovan, L.; Constantin, D.; Stanciuc, A.; Sarbu Boeti, P.; Efrimescu, I. Collagen−Based Scaffolds for Skin Tissue Engineering. *J. Med. Life* **2011**, *4*, 172−177.

(13) Duan, H.; Feng, B.; Guo, X.; Wang, J.; Zhao, L.; Zhou, G.; Liu, W.; Cao, Y.; Zhang, W. J. Engineering of Epidermis Skin Grafts Using Electrospun Nanofibrous Gelatin/Polycaprolactone Membranes. *Int. J. Nanomedicine* **2013**, *8*, 2077−2084.

(14) Hakam, M. S.; Imani, R.; Abolfathi, N.; Fakhrzadeh, H.; Sharifi, A. M. Evaluation of Fibrin-Gelatin Hydrogel as Biopaper for Application in Skin Bioprinting: An in Vitro Study. *Biomed. Mater. Eng.* **2017**, *27*, 669−682.

(15) Dai, M.; Zheng, X.; Xu, X.; Kong, X.; Li, X.; Guo, G.; Luo, F.; Zhao, X.; Wei, Y. Q.; Qian, Z. Chitosan−Alginate Sponge: Preparation and Application in Curcumin Delivery for Dermal Wound Healing in Rat. *J. Biomed. Biotechnol.* **2009**, *2009*, 1−8.

(16) Ng, K. W.; Wanivenhaus, F.; Chen, T.; Hsu, H.-C.; Allon, A. A.; Abrams, V. D.; Torzilli, P. A.; Warren, R. F.; Maher, S. A. A Novel Macroporous Poly(vinyl alcohol) Scaffold Promotes Chondrocyte Migration and Interface Formation in an In Vitro Cartilage Defect Model. *Tissue Eng., Part A* **2012**, *18*, 1273−1281.

(17) Zhou, T.; Li, X.; Li, G.; Tian, T.; Lin, S.; Shi, S.; Liao, J.; Cai, X.; Lin, Y. Injectable and Thermosensitive TGF-B1-Loaded PCEC Hydrogel System for in Vivo Cartilage Repair. *Sci. Rep.* **2017**, *7*, No. 10553.

(18) *Progress in Heritable Soft Connective Tissue Diseases*; Halper, J., Ed.; Advances in Experimental Medicine and Biology; Springer Netherlands: Dordrecht, 2014; Vol. *802*.

(19) Hirai, M.; Ohbayashi, T.; Horiguchi, M.; Okawa, K.; Hagiwara, A.; Chien, K. R.; Kita, T.; Nakamura, T. Fibulin-5/DANCE Has an Elastogenic Organizer Activity That Is Abrogated by Proteolytic Cleavage in Vivo. *J. Cell Biol.* **2007**, *176*, 1061−1071.

(20) Noori, A.; Ashrafi, S. J.; Vaez-Ghaemi, R.; Hatamian-Zaremi, A.; Webster, T. J. A Review of Fibrin and Fibrin Composites for Bone Tissue Engineering. *Int. J. Nanomed.* **2017**, *12*, 4937−4961.

(21) Mosesson, M. W. Fibrinogen and Fibrin Structure and Functions. *J. Thromb. Haemost.* **2005**, *3*, 1894−1904.

(22) GMIA. *Gelatin Handbook*; Gelatin Manufacturers Institute of America: New York, 2012; p 26.

(23) Shan, Y.-H.; Peng, L.-H.; Liu, X.; Chen, X.; Xiong, J.; Gao, J.-Q. Silk Fibroin/Gelatin Electrospun Nanofibrous Dressing Functionalized with Astragaloside IV Induces Healing and Anti-Scar Effects on Burn Wound. *Int. J. Pharm.* **2015**, *479*, 291−301.

(24) Elzoghby, A. O. Gelatin-Based Nanoparticles as Drug and Gene Delivery Systems: Reviewing Three Decades of Research. *J. Controlled Release* **2013**, *172*, 1075−1091.
(25) Sun, J.; Tan, H. Alginate-Based Biomaterials for Regenerative Medicine Applications. *Materials* **2013**, *6*, 1285−1309.
(26) Aroguz, A. Z.; Baysal, K.; Adiguzel, Z.; Baysal, B. M. Alginate/Polyoxyethylene and Alginate/Gelatin Hydrogels: Preparation, Characterization, and Application in Tissue Engineering. *Appl. Biochem. Biotechnol.* **2014**, *173*, 433−448.
(27) Balakrishnan, B.; Mohanty, M.; Umashankar, P.; Jayakrishnan, A. Evaluation of an in Situ Forming Hydrogel Wound Dressing Based on Oxidized Alginate and Gelatin. *Biomaterials* **2005**, *26*, 6335−6342.
(28) Sarhan, W. A.; Azzazy, H. M. E.; El-Sherbiny, I. M. Honey/Chitosan Nanofiber Wound Dressing Enriched with *Allium sativum* and *Cleome droserifolia*: Enhanced Antimicrobial and Wound Healing Activity. *ACS Appl. Mater. Interfaces* **2016**, *8*, 6379−6390.
(29) Muhd Julkapli, N.; Akil, H. M.; Ahmad, Z. Preparation, Properties and Applications of Chitosan-Based Biocomposites/Blend Materials: A Review. *Compos. Interfaces* **2011**, *18*, 449−507.
(30) Ridolfi, D. M.; Lemes, A. P.; de Oliveira, S.; Justo, G. Z.; Palladino, M. V.; Durán, N. Electrospun Poly(Ethylene Oxide)/Chitosan Nanofibers with Cellulose Nanocrystals as Support for Cell Culture of 3T3 Fibroblasts. *Cellulose* **2017**, *24*, 3353−3365.
(31) Vashisth, P.; Nikhil, K.; Roy, P.; Pruthi, P. A.; Singh, R. P.; Pruthi, V. A Novel Gellan−PVA Nanofibrous Scaffold for Skin Tissue Regeneration: Fabrication and Characterization. *Carbohydr. Polym.* **2016**, *136*, 851−859.
(32) Gaaz, T.; Sulong, A.; Akhtar, M.; Kadhum, A.; Mohamad, A.; Al-Amiery, A. Properties and Applications of Poly(vinyl alcohol), Halloysite Nanotubes and Their Nanocomposites. *Molecules* **2015**, *20*, 22833−22847.
(33) DeMerlis, C. C.; Schoneker, D. R. Review of the Oral Toxicity of Poly(vinyl alcohol) (PVA). *Food Chem. Toxicol.* **2003**, *41*, 319−326.
(34) Mclafferty, E.; Hendry, C.; Farley, A. The Integumentary System: Anatomy, Physiology and Function of Skin. *Nurs. Stand.* **2012**, *27*, No. 35.
(35) *Gray's Anatomy: The Anatomical Basis of Clinical Practice*, 40th ed.; Standring, S.; Gray, H., Eds.; Churchill Livingstone/Elsevier: Edinburgh, 2008.
(36) Marieb, E. N.; Mallatt, J. *Human Anatomy*, 2nd ed.; Benjamin/Cummings: Menlo Park, Calif, 1997.
(37) Semer, N. B. *Practical Plastic Surgery for Nonsurgeons*; Hanley & Belfus: Philadelphia, 2001.
(38) Kheiri, A.; Amini, S.; Javidan, A. N.; Saghafi, M. M.; Khorasani, G. The Effects of Alkanna Tinctoria Tausch on Split-Thickness Skin Graft Donor Site Management: A Randomized, Blinded Placebo-Controlled Trial. *BMC Complementary Altern. Med.* **2017**, *17*, No. 253.
(39) Pouranvari, S.; Ebrahimi, F.; Javadi, G.; Maddah, B. Chemical Cross-Linking of Chitosan/Poly(vinyl alcohol) Electrospun Nanofibers. *Mater. Tehnol.* **2016**, *50*, 663−666.
(40) Ridolfi, D. M.; Lemes, A. P.; de Oliveira, S.; Justo, G. Z.; Palladino, M. V.; Durán, N. Electrospun Poly(Ethylene Oxide)/Chitosan Nanofibers with Cellulose Nanocrystals as Support for Cell Culture of 3T3 Fibroblasts. *Cellulose* **2017**, *24*, 3353−3365.
(41) Destaye, A. G.; Lin, C.-K.; Lee, C.-K. Glutaraldehyde Vapor Cross-Linked Nanofibrous PVA Mat with in Situ Formed Silver Nanoparticles. *ACS Appl. Mater. Interfaces* **2013**, *5*, 4745−4752.
(42) Alhosseini, S. N.; Moztarzadeh, F.; Mozafari, M.; Asgari, S.; Dodel, M.; Samadikuchaksaraei, A.; Kargozar, S.; Jalali, N. Synthesis and Characterization of Electrospun Poly(vinyl alcohol) Nanofibrous Scaffolds Modified by Blending with Chitosan for Neural Tissue Engineering. *Int. J. Nanomed.* **2012**, *7*, 25−34.
(43) Droge, S.; Goss, K.-U. Effect of Sodium and Calcium Cations on the Ion-Exchange Affinity of Organic Cations for Soil Organic Matter. *Environ. Sci. Technol.* **2012**, *46*, 5894−5901.
(44) Rath, B.; Klameth, L.; Plangger, A.; Hochmair, M.; Ulsperger, E.; Huk, I.; Zeillinger, R.; Hamilton, G. Expression of Proteolytic Enzymes by Small Cell Lung Cancer Circulating Tumor Cell Lines. *Cancers* **2019**, *11*, No. 114.
(45) Gaspar, A.; Moldovan, L.; Constantin, D.; Stanciuc, A. M.; Sarbu Boeti, P. M.; Efrimescu, I. C. Collagen-Based Scaffolds for Skin Tissue Engineering. *J. Med. Life* **2011**, *4*, 172−177.
(46) *Collagen: Structure and Mechanics*; Fratzl, P., Ed.; Springer: New York, 2008.
(47) Baniasadi, M.; Minary-Jolandan, M. Alginate-Collagen Fibril Composite Hydrogel. *Materials* **2015**, *8*, 799−814.
(48) Silva, S. M.; Braga, C. R.; Fook, M. V.; Raposo, C. M.; Carvalho, L. H.; Canedo, E. L. Application of Infrared Spectroscopy to Analysis of Chitosan/Clay Nanocomposites. In *Infrared Spectroscopy-Materials Science, Engineering and Technology*; InTech, 2012.
(49) Osuna, Y.; Gregorio-Jauregui, K. M.; Gaona-Lozano, J. G.; de la Garza-Rodríguez, I. M.; Ilyna, A.; Barriga-Castro, E. D.; Saade, H.; López, R. G. Chitosan-Coated Magnetic Nanoparticles with Low Chitosan Content Prepared in One-Step. *J. Nanomater.* **2012**, *2012*, 1−7.
(50) Skopinska-Wisniewska, J.; Kuderko, J.; Bajek, A.; Maj, M.; Sionkowska, A.; Ziegler-Borowska, M. Collagen/Elastin Hydrogels Cross-Linked by Squaric Acid. *Mater. Sci. Eng., C* **2016**, *60*, 100−108.
(51) Silva, R.; Singh, R.; Sarker, B.; Papageorgiou, D. G.; Juhasz-Bortuzzo, J. A.; Roether, J. A.; Cicha, I.; Kaschta, J.; Schubert, D. W.; Chrissafis, K.; et al. Hydrogel Matrices Based on Elastin and Alginate for Tissue Engineering Applications. *Int. J. Biol. Macromol.* **2018**, *114*, 614−625.
(52) Maria, C. Application of FTIR Spectroscopy in Environmental Studies. In *Advanced Aspects of Spectroscopy*; Akhyar Farrukh, M., Ed.; InTech, 2012.
(53) Rouquerol, J.; Avnir, D.; Fairbridge, C. W.; Everett, D. H.; Haynes, J. H.; Pernicone, N.; Ramsay, J. D. F.; Sing, K. S. W.; Unger, K. K. Recommendations for the Characterization of Porous Solids. *Pure Appl. Chem.* **1994**, *66*, 1739−1758.
(54) Arkoun, M.; Daigle, F.; Heuzey, M.-C.; Ajji, A. Antibacterial Electrospun Chitosan-based Nanofibers: A Bacterial Membrane Perforator. *Food Sci. Nutr.* **2017**, *5*, 865−874.
(55) Silhavy, T. J.; Kahne, D.; Walker, S. The Bacterial Cell Envelope. *Cold Spring Harbor Perspect. Biol.* **2010**, *2*, No. a000182.
(56) Nikaido, H. Multidrug Efflux Pumps of Gram-Negative Bacteria. *J. Bacteriol.* **1996**, *178*, 5853−5859.
(57) Helander, I. M.; Nurmiaho-Lassila, E.-L.; Ahvenainen, R.; Rhoades, J.; Roller, S. Chitosan Disrupts the Barrier Properties of the Outer Membrane of Gram-Negative Bacteria. *Int. J. Food Microbiol.* **2001**, *71*, 235−244.
(58) Li, W.; Li, X.; Chen, Y.; Li, X.; Deng, H.; Wang, T.; Huang, R.; Fan, G. Poly(Vinyl Alcohol)/Sodium Alginate/Layered Silicate Based Nanofibrous Mats for Bacterial Inhibition. *Carbohydr. Polym.* **2013**, *92*, 2232−2238.
(59) Kawai, F.; Hu, X. Biochemistry of Microbial Poly(vinyl alcohol) Degradation. *Appl. Microbiol. Biotechnol.* **2009**, *84*, 227−237.
(60) Aljarah, A. K.; Al-Saadi, A. H.; Auda, N. A. ELK1 Gene Transfection Effect in Prostate Cancer Cell Line Proliferation Activity. *Advances in Life Science and Technology* **2014**, *26*, 94.
(61) Maisani, M.; Ziane, S.; Ehret, C.; Levesque, L.; Siadous, R.; Le Meins, J.-F.; Chevallier, P.; Barthélémy, P.; De Oliveira, H.; Amédée, J.; et al. A New Composite Hydrogel Combining the Biological Properties of Collagen with the Mechanical Properties of a Supramolecular Scaffold for Bone Tissue Engineering. *J. Tissue Eng. Regener. Med.* **2018**, *12*, e1489−e1500.
(62) Edgar, S.; Hopley, B.; Genovese, L.; Sibilla, S.; Laight, D.; Shute, J. Effects of Collagen-Derived Bioactive Peptides and Natural Antioxidant Compounds on Proliferation and Matrix Protein Synthesis by Cultured Normal Human Dermal Fibroblasts. *Sci. Rep.* **2018**, *8*, No. 10474.
(63) Sarker, B.; Singh, R.; Silva, R.; Roether, J. A.; Kaschta, J.; Detsch, R.; Boccaccini, A. R. Evaluation of fibroblasts adhesion and proliferation on alginate-gelatin crosslinked hydrogel. *PLoS One* **2014**, *9*, No. e107952.

https://dx.doi.org/10.1021/acsomega.9b02832
ACS Omega 2020, 5, 2133−2147

(64) Vandrovcová, M.; Douglas, T.; Hauk, D.; Grössner-Schreiber, B.; Wiltfang, J.; Bacakova, L.; Warnke, P. H. Influence of Collagen and Chondroitin Sulfate (CS) Coatings on Poly-(Lactide-Co-Glycolide)-(PLGA) on MG 63 Osteoblast-like Cells. *Physiol. Res.* **2011**, *60*, No. 797.
(65) Wang, L.; Stegemann, J. P. Thermogelling Chitosan and Collagen Composite Hydrogels Initiated with β-Glycerophosphate for Bone Tissue Engineering. *Biomaterials* **2010**, *31*, 3976−3985.
(66) Davidenko, N.; Schuster, C. F.; Bax, D. V.; Farndale, R. W.; Hamaia, S.; Best, S. M.; Cameron, R. E. Evaluation of Cell Binding to Collagen and Gelatin: A Study of the Effect of 2D and 3D Architecture and Surface Chemistry. *J. Mater. Sci. Mater. Med.* **2016**, *27*, No. 148.
(67) Lee, P.; Yeo, G. C.; Weiss, A. S. A Cell Adhesive Peptide from Tropoelastin Promotes Sequential Cell Attachment and Spreading via Distinct Receptors. *FEBS J.* **2017**, *284*, 2216−2230.
(68) Huang, C.-Y.; Hu, K.-H.; Wei, Z.-H. Comparison of Cell Behavior on Pva/Pva-Gelatin Electrospun Nanofibers with Random and Aligned Configuration. *Sci. Rep.* **2016**, *6*, No. 37960.
(69) Mohanapriya, S.; Raj, V. Tuning biological properties of poly(vinyl alcohol) with amino acids and studying its influence on osteoblastic cell adhesion. *Mater. Sci. Eng., C* **2018**, 70−82.
(70) Kim, K. S.; Lee, J. H.; Ahn, H. H.; Lee, J. Y.; Khang, G.; Lee, B.; Lee, H. B.; Kim, M. S. The Osteogenic Differentiation of Rat Muscle-Derived Stem Cells in Vivo within in Situ-Forming Chitosan Scaffolds. *Biomaterials* **2008**, *29*, 4420−4428.
(71) Bellis, S. L. Advantages of RGD Peptides for Directing Cell Association with Biomaterials. *Biomaterials* **2011**, *32*, 4205−4210.
(72) Zhang, X.; Wang, H.; Ma, X.; Adila, A.; Wang, B.; Liu, F.; Chen, B.; Wang, C.; Ma, Y. Preservation of the Cardiac Function in Infarcted Rat Hearts by the Transplantation of Adipose-Derived Stem Cells with Injectable Fibrin Scaffolds. *Exp. Biol. Med.* **2010**, *235*, 1505−1515.
(73) Ryu, J.; Kim, I.; Cho, S.; Cho, M.; Hwang, K.; Piao, H.; Piao, S.; Lim, S.; Hong, Y.; Choi, C. Implantation of Bone Marrow Mononuclear Cells Using Injectable Fibrin Matrix Enhances Neovascularization in Infarcted Myocardium. *Biomaterials* **2005**, *26*, 319−326.
(74) Hong, H.; Stegemann, J. P. 2D and 3D Collagen and Fibrin Biopolymers Promote Specific ECM and Integrin Gene Expression by Vascular Smooth Muscle Cells. *J. Biomater. Sci. Polym. Ed.* **2008**, *19*, 1279−1293.
(75) Wiegand, I.; Hilpert, K.; Hancock, R. E. W. Agar and Broth Dilution Methods to Determine the Minimal Inhibitory Concentration (MIC) of Antimicrobial Substances. *Nat. Protoc.* **2008**, *3*, 163−175.
(76) Misra, R.; Sahoo, S. K. Antibacterial Activity of Doxycycline-Loaded Nanoparticles. In *Methods in Enzymology*; Elsevier, 2012; Vol. *509*, pp 61−85.

https://dx.doi.org/10.1021/acsomega.9b02832
ACS Omega 2020, 5, 2133−2147